Nonlinear Adaptive Burn Control and Optimal Control Allocation of Over-Actuated Two-Temperature Plasmas

Vincent Graber and Eugenio Schuster

Abstract— **Tokamaks are reactors that produce energy from the fusion, or merging, of atomic particles. A suitable reaction rate is achieved by heating a gas of charged particles (free ions and electrons), or plasma, to extreme temperatures. From the fusion of deuterium and tritium ions, a burning plasma produces alpha particles that contribute to the heating of the plasma. Burning plasmas are highly nonlinear systems that require careful regulation of temperature and density, or burn control, to reach desirable operating points. Once constructed, ITER will be the first tokamak designed for burning plasmas. In this work, a Lyapunov-based burn controller is developed using a full zero-dimensional nonlinear model. An adaptive estimator manages the presence of uncertain model parameters. The control objective is to stabilize equilibria despite model nonlinearity and uncertainty. Density is regulated through the injection of fuel pellets. For ITER, the temperature of the ions may differ significantly from that of the electrons in the plasma core. Therefore, the proposed controller considers separate response models for ion and electron energies. For energy control, the controller commands two virtual control efforts: the external ion heating and the external electron heating. To satisfy these two virtual control efforts, ITER will have access to ion cyclotron heating, electron cyclotron heating and two neutral beam injectors. With more actuators than virtual control efforts, the two-temperature plasma system is over-actuated. Actuator redundancy is resolved by constructing an optimal control allocator that considers actuator saturation and rate limits. A simulation study demonstrates the capability of the adaptive control and control allocation algorithms.**

I. INTRODUCTION

The fusion of deuterium (D) and tritium (T) fuel ions creates an energetic alpha particle and a neutron. A toroidal device, known as a tokamak [1], produces energy by magnetically confining an ionized gas, or plasma, at extreme temperatures where the DT ions can overcome their mutual Coulomb repulsion and fuse. Under the magnetic confinement, the charged alpha particles are trapped and their kinetic energies are absorbed by the plasma, providing the desirable self-heating quality of burning plasmas. The neutrons escape the confinement, and their energy is converted to electricity. ITER, the prospective first burning-plasma tokamak, will have access to ion cyclotron (IC), electron cyclotron (EC) and neutral beam (NB) heating systems [2] . Pellet injectors will provide fuel replenishment. To achieve high fusion to auxiliary power ratios, burn controllers will be employed to determine the external heating and fueling requirements.

Previous work [3], [4] on nonlinear burn control algorithms used approximated one-temperature models. More recently, the authors proposed a nonlinear control based on a two-temperature model to better represent the plasma conditions anticipated in ITER [5]. Transport codes predict that for ITER the electron temperature will be generally 20% higher than the ion temperature in the plasma core [6]. Fusion alpha particles are one of the primary causes of the temperature difference. Only a small percentage of alpha particle power is delivered to the ions. With the rest deposited into the electrons, the electron temperature will typically be higher than the ion temperature. The large ion-to-electron mass ratio makes collisional energy exchange between the two species inefficient, slowing ion-electron thermal relaxation [7].

As a first approach to the problem, the model considered in [5] made the simplifying assumption that the ratio of ion and electron energies was constant. After applying this assumption to the total plasma energy response model, the control design derived one virtual control law for the total external heating. While the ion energy was directly controlled, the electron energy evolved passively due to the fixed proportionality constant. In contrast, the controller designed in this work avoids both the one-temperature and the fixed energy ratio assumptions by considering separate ion and electron response models. The proposed control design independently regulates ion and electron energies with the use of separate virtual control laws for external ion heating and external electron heating. Lyapunov techniques [8] were applied to formulate the stabilizing control laws. Adaptive estimation is used to account for uncertain model parameters.

The controller's commanded virtual control efforts for ion and electron heating need to be met using the available heating systems. With more heating systems (IC, EC, NB) than commanded virtual control efforts, the system is over-actuated. This actuator redundancy is resolved using a control allocation (CA) module that optimally maps the commanded efforts to the control inputs. The CA module is separate from the high level plasma control algorithm. There are benefits to using this modular scheme over an optimal controller that determines the control inputs directly. Actuator constraints can be better handled and actuator reconfigurations do not require alteration of the virtual control laws [9]. The proposed CA module solves a convex quadratic program that considers actuator saturation and rate limits.

This paper is divided as follows. The plasma model is covered in Section II. In Section III, control objectives are drawn. The adaptive controller is designed in Section IV. The CA module is presented in Section V. In Section VI, the controller and CA module are studied with simulations. Conclusions and future work are stated in Section VII.

This work was supported in part by the U.S. Department of Energy (DE-SC0010661). V. Graber (graber@lehigh.edu) and E. Schuster are with the Department of Mechanical Engineering and Mechanics, Lehigh University, Bethlehem, PA 18015, USA.

II. THE TWO-TEMPERATURE PLASMA MODEL

In this volume-averaged model, the particle densities of deuterium, tritium, alpha particles and impurities are n_α, n_D, n_T and n_I, respectively. Expressing each term in units of $\mathrm{m}^{-3}\mathrm{s}^{-1}$, the density response models for each species are

$$\dot{n}_D = -\frac{n_D}{\tau_D} - S_\alpha + S_D, \quad \dot{n}_\alpha = -\frac{n_\alpha}{\tau_\alpha} + S_\alpha, \tag{1}$$

$$\dot{n}_T = -\frac{n_T}{\tau_T} - S_\alpha + S_T, \quad \dot{n}_I = -\frac{n_I}{\tau_I} + S_I^{sp}. \tag{2}$$

The controlled injection rates of deuterium and tritium are S_D and S_T, respectively. Transport out of the plasma is modeled using particle confinement times τ_α, τ_D, τ_T and τ_I. The fusion reaction rate density, S_α, can be expressed in terms of the DT reactivity, $\langle\sigma\nu\rangle$, such that $S_\alpha = n_D n_T \langle\sigma\nu\rangle$. Quasi-neutrality, which demands equal numbers of electrons and protons in the plasma, defines the electron density as $n_e = n_H + 2n_\alpha + Z_I n_I$ where $n_H = n_D + n_T$ and Z_I is the average atomic number of the impurity ions. The total plasma density and the tritium fraction are defined, respectively, as

$$n = n_H + n_\alpha + n_I + n_e, \qquad \gamma = n_T/n_H. \tag{3}$$

Erosion of the vessel walls results in the absorption of impurity ions into the plasma. The impurity sputtering source is expressed as $S_I^{sp} = f_I^{sp}(n/\tau_I + \dot{n})$, where f_I^{sp} is the sputtering fraction. Although models in previous work [4], [5] included DT recycling due to plasma-wall interactions, this work omits it for brevity. The control algorithm developed in Section IV can easily be extended to a model with recycling.

The plasma ions and electrons have unique temperatures T_i and T_e, respectively. The total plasma energy, E, is the sum of the ion energy, E_i, and the electron energy, E_e. Therefore, $E = E_i + E_e = \frac{3}{2}(n_H + n_\alpha + n_I)T_i + \frac{3}{2}n_e T_e$. The separate ion and electron energy response models are

$$\dot{E}_i = -\frac{E_i}{\tau_{E,i}} + \phi_\alpha P_\alpha + P_{ei} + P_{aux,i}, \tag{4}$$

$$\dot{E}_e = -\frac{E_e}{\tau_{E,e}} + (1-\phi_\alpha)P_\alpha - P_{ei} - P_{br} + P_{oh} + P_{aux,e}, \tag{5}$$

where P_α is the alpha particle heating from fusion reactions, ϕ_α is the fraction of P_α deposited into the plasma ions, P_{br} is the bremsstrahlung radiation losses, P_{oh} is the ohmic heating, P_{ei} is the ion-electron collisional power exchange, $P_{aux,i}$ and $P_{aux,e}$ are the controlled external heating delivered to the ions and electrons, respectively. Each term has units of Wm^{-3}. The energy confinement times are $\tau_{E,i}$ and $\tau_{E,e}$.

Each fusion reaction produces one alpha particle with $Q_\alpha = 3.52$ MeV of kinetic energy. Therefore, $P_\alpha = Q_\alpha S_\alpha$. With T_i expressed in keV, the DT reactivity [10] is given by

$$\langle\sigma\nu\rangle = C_1\omega\sqrt{\xi/(m_r c^2 T_i^3)}e^{-3\xi}, \quad \xi = (B_G^2/4\omega)^{1/3} \tag{6}$$

$$\omega = T_i\left[1 - \frac{T_i(C_2 + T_i(C_4 + T_i C_6))}{1 + T_i(C_3 + T_i(C_5 + T_i C_7))}\right]^{-1}, \tag{7}$$

where and B_G, $m_r c^2$ and C_j for $j \in \{1, ..., 7\}$ are constants.

While the DT reactivity depends on ion temperature, the radiation losses, $P_{br} = 5.5 \times 10^{-37} Z_{eff} n_e^2 \sqrt{T_e}$, and ohmic heating, $P_{oh} = 2.8 \times 10^{-9} Z_{eff} I_p^2 a^{-4} T_e^{-3/2}$, depend on electron temperature (expressed in keV). The plasma current and minor radius are I_p and a. The effective atomic number is $Z_{eff} = (n_H + 4n_\alpha + Z_I^2 n_I)/n_e$. Bremsstrahlung radiation does not depend on T_i because the light electrons accelerate and radiate much more than the heavy ions [1].

The power exchange between ions and electrons is

$$P_{ei} = \frac{3}{2}n_e\frac{T_e - T_i}{\tau_{ei}}, \quad \tau_{ei} = \frac{3\pi\sqrt{2\pi}\varepsilon_0^2 T_e^{3/2}}{e^4 m_e^{1/2}\ln\Lambda_e}\sum_{ions}\frac{m_i}{n_i Z_i^2}, \tag{8}$$

where τ_{ei} is the energy relaxation time [11]. In (8), $e = 1.622 \times 10^{-19}$C, $m_e = 9.1096 \times 10^{-31}$kg, $\varepsilon_0 = 8.854 \times 10^{-12}$F/m and T_e is expressed in J. The natural logarithm is given by $\Lambda_k = 1.24 \times 10^7 T_k^{3/2}/(n_e^{1/2} Z_{eff}^2)$ for $k \in \{i, e\}$.

Fast ions, such as fusion-born alpha particles or injected neutral beam particles, deposit fractions ϕ_f and $\bar{\phi}_f \triangleq (1-\phi_f)$ for $f \in \{\alpha, nbi\}$ of their energy into the plasma ions and electrons. As a fast ion collides with the surrounding plasma particles [1], it loses energy, ε_f for $f \in \{\alpha, nbi\}$, at a rate of

$$\frac{d\varepsilon_f}{dt} = -D\varepsilon_f - D\varepsilon_f\left(\frac{\varepsilon_c}{\varepsilon_f}\right)^{3/2} \equiv -P_{fe} - P_{fi}, \tag{9}$$

where $D = m_e^{1/2} e^4 n_e Z_f^2 \ln\Lambda_e/(3\sqrt{2}\pi^{3/2}\varepsilon_0^2 m_f T_e^{3/2})$. The fast ion's charge and mass are Z_f and m_f for $f \in \{\alpha, nbi\}$. The first and second terms of (9) represent the power going to the electrons (P_{fe}) and ions (P_{fi}), respectively. At high energies [12], the fast ions primarily heat the electrons. As fast ions slow down, more of their energy goes to the ions. The electron and ion heating are equal at the critical energy,

$$\varepsilon_c = m_e^{-1/3} A_f \frac{T_e}{n_e^{2/3}}\left(\frac{3\sqrt{\pi}\ln\Lambda_i}{4\ln\Lambda_e}\right)^{2/3}\left(\sum_{ions}\frac{n_i Z_i^2}{A_i}\right), \tag{10}$$

where A_f for $f \in \{\alpha, nbi\}$ and A_i for $i \in \{\alpha, D, T, I\}$ are, respectively, the atomic mass of the fast ion and plasma ions (m_e is in amu). By solving for D in (9) and substituting it into the definition of P_{fi}, P_{fi} can be expressed in terms of $d\varepsilon_f/dt$. Then, the total energy delivered to the ions can be found by integrating P_{fi} in time from zero to the time it takes for the fast ion to lose all of its energy, t_f. The ion-heating fraction, ϕ_f for $f \in \{\alpha, nbi\}$, is this integral divided by the the fast ion's initial kinetic energy, ε_{f_0} for $f \in \{\alpha, nbi\}$:

$$\begin{aligned}\phi_f &\triangleq \frac{1}{\varepsilon_{f_0}}\int_0^{t_f} P_{fi}dt = \frac{1}{\varepsilon_{f_0}}\int_0^{t_f}\frac{-\varepsilon_c^{3/2}}{\varepsilon_f^{3/2}+\varepsilon_c^{3/2}}\frac{d\varepsilon_f}{dt}dt \\ &= \frac{\varepsilon_c^{3/2}}{\varepsilon_{f_0}}\int_{\varepsilon_{f_0}}^{0}\frac{-d\varepsilon_f}{\varepsilon_f^{3/2}+\varepsilon_c^{3/2}} = \frac{1}{\varepsilon_{f_0}}\int_0^{\varepsilon_{f_0}}\frac{d\varepsilon_f}{(\varepsilon_f/\varepsilon_c)^{3/2}+1}.\end{aligned} \tag{11}$$

With the change in variables $x = \varepsilon_f/\varepsilon_c$ and $x_0 = \varepsilon_{f_0}/\varepsilon_c$,

$$\begin{aligned}\phi_f &= \frac{\varepsilon_c}{\varepsilon_{f_0}}\int_0^{\varepsilon_{f_0}/\varepsilon_c}\frac{d(\varepsilon_f/\varepsilon_c)}{(\varepsilon_f/\varepsilon_c)^{3/2}+1} = \frac{1}{x_0}\int_0^{x_0}\frac{dx}{x^{3/2}+1} \\ &= \frac{1}{x_0}\left[\frac{1}{3}\ln\frac{1-x_0^{1/2}+x_0}{(1+x_0^{1/2})^2} + \frac{2}{\sqrt{3}}\left(\arctan\frac{2x_0^{1/2}-1}{\sqrt{3}} + \frac{\pi}{6}\right)\right].\end{aligned} \tag{12}$$

The fraction of P_α delivered to the ions, ϕ_α in (4) and (5), is calculated using (10) and (12) with $\varepsilon_{\alpha_0} = Q_\alpha$ and $A_\alpha = 4$.

The expression for the global energy confinement time is

$$\tau_E = H\tau_E^{sc} = HKP^{-0.69}V^{-0.69}n_{e_{19}}^{0.41}, \tag{13}$$

where $K = 0.0562 I_p^{0.93} B_T^{0.15} M^{0.19} R^{1.97} \epsilon^{0.58} \kappa^{0.78}$, H is a constant that depends on plasma's confinement quality, B_T is the toroidal field, R is the plasma major radius, $\epsilon = a/R$, $M = 3\gamma + 2(1-\gamma)$, κ is the vertical elongation at 95% flux surface, $P = P_{aux,i} + P_{aux,e} - P_{br} + P_\alpha + P_{oh}$ is the total power in MWm^{-3}, V is the plasma volume, and n_e is in units of $10^{19}\mathrm{m}^{-3}$ [13]. In ITER, I_p, B_T, R, a, κ and V have values 15 MA, 5.3 T, 6.2 m, 2 m, 1.7 and 837 m^3, respectively. The particle confinement times are proportional to global energy confinement time: $\tau_h = k_h \tau_E$ for $h \in \{\alpha, D, T, I\}$. Similarly, $\zeta_i = \tau_{E,i}/\tau_E$ and $\zeta_e = \tau_{E,e}/\tau_E$ are constant.

The parameters H, ζ_i, ζ_e, k_D, k_T, k_α, k_I and f_I^{sp} are uncertain, and they are grouped into the nominal uncertainty vector θ such that (1), (2), (4) and (5) can be rewritten as

$$\begin{aligned}
\dot{E}_i &= -\theta_1 \frac{E_i}{\tau_E^{sc}} + \phi_\alpha P_\alpha + P_{ei} + P_{aux,i},\\
\dot{E}_e &= -\theta_2 \frac{E_e}{\tau_E^{sc}} + (1-\phi_\alpha)P_\alpha - P_{ei} - P_{br} + P_{oh} + P_{aux,e},\\
\dot{n}_\alpha &= -\theta_3 \frac{n_\alpha}{\tau_E^{sc}} + S_\alpha,\\
\dot{n}_D &= -\theta_4 \frac{n_D}{\tau_E^{sc}} - S_\alpha + S_{D,}\\
\dot{n}_T &= -\theta_5 \frac{n_T}{\tau_E^{sc}} - S_\alpha + S_T,\\
\dot{n}_I &= -\theta_6 \frac{n_I}{\tau_E^{sc}} + \theta_7 \frac{n}{\tau_E^{sc}} + \theta_8 \dot{n},
\end{aligned} \tag{14}$$

where θ_i is the i^{th} element of θ. The elements of θ can be easily inferred from (1), (2), (4), (5) and (14).

III. BURN CONTROL OBJECTIVES

The controller is designed to track equilibria defined by system (14) at steady-state. With six states (with desired values $\bar{E}_i$, $\bar{E}_e$, $\bar{n}_\alpha$, $\bar{n}_D$, $\bar{n}_T$, $\bar{n}_I$) and four virtual control efforts ($\bar{P}_{aux,i}$, $\bar{P}_{aux,e}$, $\bar{S}_D$, $\bar{S}_T$), the system of six equations is solved by predefining $\bar{E}_i$, $\bar{E}_e$, $\bar{n}$ and $\bar{\gamma}$. Deviations of states from their desired values are $\tilde{E}_i = E_i - \bar{E}_i$, $\tilde{E}_e = E_e - \bar{E}_e$, $\tilde{n}_\alpha = n_\alpha - \bar{n}_\alpha$, $\tilde{n}_D = n_D - \bar{n}_D$, $\tilde{n}_T = n_T - \bar{n}_T$ and $\tilde{n}_I = n_I - \bar{n}_I$. The control objective is to drive the deviations in the system,

$$\begin{aligned}
\dot{\tilde{E}}_i &= -\theta_1 \frac{\bar{E}_i + \tilde{E}_i}{\tau_E^{sc}} + \phi_\alpha P_\alpha + P_{ei} + P_{aux,i},\\
\dot{\tilde{E}}_e &= -\theta_2 \frac{\bar{E}_e + \tilde{E}_e}{\tau_E^{sc}} + (1-\phi_\alpha)P_\alpha - P_{ei} - P_{br} + P_{oh} + P_{aux,e},\\
\dot{\tilde{n}}_\alpha &= -\theta_3 \frac{\bar{n}_\alpha + \tilde{n}_\alpha}{\tau_E^{sc}} + S_\alpha,\\
\dot{\tilde{n}}_D &= -\theta_4 \frac{\bar{n}_D + \tilde{n}_D}{\tau_E^{sc}} - S_\alpha + S_D,\\
\dot{\tilde{n}}_T &= -\theta_5 \frac{\bar{n}_T + \tilde{n}_T}{\tau_E^{sc}} - S_\alpha + S_T,\\
\dot{\tilde{n}}_I &= -\theta_6 \frac{\bar{n}_I + \tilde{n}_I}{\tau_E^{sc}} + \theta_7 \frac{\bar{n} + \tilde{n}}{\tau_E^{sc}} + \theta_8 \dot{\tilde{n}},
\end{aligned} \tag{15}$$

to zero despite model uncertainty. This is accomplished by developing adaptive control laws from a Lyapunov function.

IV. ADAPTIVE BURN CONTROL ALGORITHM

Control laws for heating, $P_{aux,i}$ and $P_{aux,e}$, and fueling, S_D and S_T, are developed using the Lyapunov function

$$V = k_i^2 \tilde{E}_i^2 + k_e^2 \tilde{E}_e^2 + k_\gamma^2 \tilde{\gamma}^2 + \tilde{n}^2 + \tilde{\theta}^T \Gamma^{-1} \tilde{\theta}, \tag{16}$$

where Γ is a positive definite matrix, and k_i, k_e and k_γ are positive constants. The vector $\tilde{\theta}$ is the online estimation error of nominal θ. The controller's current estimation of nominal θ is $\hat{\theta}$. Therefore, $\tilde{\theta} = \hat{\theta} - \theta$. The time derivative of (16) is

$$\dot{V} = k_i^2 \tilde{E}_i \dot{\tilde{E}}_i + k_e^2 \tilde{E}_e \dot{\tilde{E}}_e + k_\gamma^2 \tilde{\gamma} \dot{\tilde{\gamma}} + \tilde{n} \dot{\tilde{n}} + \tilde{\theta}^T \Gamma^{-1} \dot{\tilde{\theta}}. \tag{17}$$

Recalling (3) and (15), the derivatives $\dot{\tilde{n}}$ and $\dot{\tilde{\gamma}}$ are

$$\begin{aligned}
\dot{\tilde{n}} &= 3\dot{\tilde{n}}_\alpha + 2\dot{\tilde{n}}_T + 2\dot{\tilde{n}}_D + (Z_I+1)\dot{\tilde{n}}_I\\
&= -3\theta_3 \frac{n_\alpha}{\tau_E^{sc}} - 2\theta_5 \frac{n_T}{\tau_E^{sc}} - 2\theta_4 \frac{n_D}{\tau_E^{sc}} - (Z_I+1)\theta_6 \frac{n_I}{\tau_E^{sc}} - S_\alpha\\
&\quad + 2S_D + 2S_T + (Z_I+1)\theta_7 \frac{n}{\tau_E^{sc}} + (Z_I+1)\theta_8 \dot{n},
\end{aligned} \tag{18}$$

$$\begin{aligned}
\dot{\tilde{\gamma}} &= \frac{\dot{n}_T n_H - n_T \dot{n}_H}{n_H^2} = \frac{\dot{n}_T}{n_H} - \gamma\left(\frac{\dot{n}_D + \dot{n}_T}{n_H}\right) = \frac{1}{n_H}\Bigg[S_T - S_\alpha\\
&\quad - \theta_5 \frac{n_T}{\tau_E^{sc}} - \gamma\Big(S_D + S_T - \theta_4 \frac{n_D}{\tau_E^{sc}} - \theta_5 \frac{n_T}{\tau_E^{sc}} - 2S_\alpha\Big)\Bigg].
\end{aligned} \tag{19}$$

Substituting expressions for $\dot{\tilde{E}}_i$, $\dot{\tilde{E}}_e$, $\dot{\tilde{n}}$ and $\dot{\tilde{\gamma}}$ into (17) gives

$$\begin{aligned}
\dot{V} &= k_i^2 \tilde{E}_i \left[P_{aux,i} - \theta_1 \frac{\bar{E}_i}{\tau_E^{sc}} - \theta_1 \frac{\tilde{E}_i}{\tau_E^{sc}} + \phi_\alpha P_\alpha + P_{ei}\right]\\
&\quad + k_e^2 \tilde{E}_e \left[P_{aux,e} - \theta_2 \frac{\bar{E}_e}{\tau_E^{sc}} - \theta_2 \frac{\tilde{E}_e}{\tau_E^{sc}} + (1-\phi_\alpha)P_\alpha - P_{ei}\right.\\
&\quad \left. - P_{br} + P_{oh}\right] + \frac{k_\gamma^2}{n_H} \tilde{\gamma}\left[S_T - S_\alpha - \theta_5 \frac{n_T}{\tau_E^{sc}} - \gamma\Big(S_D\right.\\
&\quad \left. + S_T - \theta_4 \frac{n_D}{\tau_E^{sc}} - \theta_5 \frac{n_T}{\tau_E^{sc}} - 2S_\alpha\Big)\right] + \tilde{n}\left[2S_D + 2S_T\right.\\
&\quad \left. - 3\theta_3 \frac{n_\alpha}{\tau_E^{sc}} - 2\theta_5 \frac{n_T}{\tau_E^{sc}} - 2\theta_4 \frac{n_D}{\tau_E^{sc}} - (Z_I+1)\theta_6 \frac{n_I}{\tau_E^{sc}} - S_\alpha\right.\\
&\quad \left. + (Z_I+1)\theta_7 \frac{n}{\tau_E^{sc}} + (Z_I+1)\theta_8 \dot{n}\right] + \tilde{\theta}^T \Gamma^{-1} \dot{\tilde{\theta}}.
\end{aligned} \tag{20}$$

With application of the certainty equivalence principle (assume $\hat{\theta} = \theta$) [14], the control laws are taken as

$$P_{aux,i} = \hat{\theta}_1 \frac{\bar{E}_i}{\tau_E^{sc}} - \phi_\alpha P_\alpha - P_{ei}, \tag{21}$$

$$P_{aux,e} = \hat{\theta}_2 \frac{\bar{E}_e}{\tau_E^{sc}} - (1-\phi_\alpha)P_\alpha + P_{ei} + P_{br} - P_{oh}, \tag{22}$$

$$\begin{aligned}
S_D &= \frac{1}{2}\Bigg[3\hat{\theta}_3 \frac{n_\alpha}{\tau_E^{sc}} + 2\hat{\theta}_4 \frac{n_D}{\tau_E^{sc}} + 2\hat{\theta}_5 \frac{n_T}{\tau_E^{sc}} + (Z_I+1)\hat{\theta}_6 \frac{n_I}{\tau_E^{sc}}\\
&\quad + S_\alpha - 2S_T - (Z_I+1)\left(\hat{\theta}_7 \frac{n}{\tau_E^{sc}} + \hat{\theta}_8 \dot{n}\right) - K_N \tilde{n}\Bigg],
\end{aligned} \tag{23}$$

$$\begin{aligned}
S_T &= \hat{\theta}_5 \frac{n_T}{\tau_E^{sc}} + S_\alpha + \gamma\Bigg[\frac{3}{2}\left(\hat{\theta}_3 \frac{n_\alpha}{\tau_E^{sc}} - S_\alpha\right) + \frac{(Z_I+1)}{2}\hat{\theta}_6 \frac{n_I}{\tau_E^{sc}}\\
&\quad - \frac{(Z_I+1)}{2}\left(\hat{\theta}_7 \frac{n}{\tau_E^{sc}} + \hat{\theta}_8 \dot{n}\right) - \frac{K_N}{2}\tilde{n}\Bigg] - K_T \tilde{\gamma},
\end{aligned} \tag{24}$$

where K_N and K_T are positive constants. Application of (21), (22), (23) and (24) transforms (20) to

$$\dot{V} = -\frac{k_i^2\tilde{E}_i^2}{\tau_E^{sc}}\theta_1 - \frac{k_e^2\tilde{E}_e^2}{\tau_E^{sc}}\theta_2 + k_i^2\tilde{E}_i\frac{\bar{E}_i}{\tau_E^{sc}}\tilde{\theta}_1 + k_e^2\tilde{E}_e\frac{\bar{E}_e}{\tau_E^{sc}}\tilde{\theta}_2 + 3\tilde{n}\frac{n_\alpha}{\tau_E^{sc}}\tilde{\theta}_3 + \left(2\tilde{n} - \frac{k_\gamma^2\tilde{\gamma}}{n_H}\gamma\right)\frac{n_D}{\tau_E^{sc}}\tilde{\theta}_4 + \tilde{n}(Z_I+1)\frac{n_I}{\tau_E^{sc}}\tilde{\theta}_6 + \left(2\tilde{n} - (\gamma-1)\frac{k_\gamma^2\tilde{\gamma}}{n_H}\right)\frac{n_T}{\tau_E^{sc}}\tilde{\theta}_5 - (Z_I+1)\tilde{n}\frac{n}{\tau_E^{sc}}\tilde{\theta}_7 - (Z_I+1)\tilde{n}\dot{n}\tilde{\theta}_8 - K_T\frac{k_\gamma^2\tilde{\gamma}^2}{n_H} - K_N\tilde{n}^2 + \tilde{\theta}^T\Gamma^{-1}\dot{\tilde{\theta}}. \quad (25)$$

The following stability condition is attained when $\tilde{\theta} = 0$:

$$\dot{V} = -\frac{k_i^2\tilde{E}_i^2}{\tau_E^{sc}}\theta_1 - \frac{k_e^2\tilde{E}_e^2}{\tau_E^{sc}}\theta_2 - K_T\frac{k_\gamma^2\tilde{\gamma}^2}{n_H} - K_N\tilde{n}^2 \leq 0. \quad (26)$$

Since parameters are usually unknown ($\hat{\theta} \neq \theta$), the controller needs to estimate θ online for (26) to hold. Adaptive law,

$$\dot{\hat{\theta}} \approx \dot{\tilde{\theta}} = \Gamma \begin{bmatrix} -(\bar{E}_i/\tau_E^{sc})k_i^2\tilde{E}_i \\ -(\bar{E}_e/\tau_E^{sc})k_e^2\tilde{E}_e \\ -3\tilde{n}(n_\alpha/\tau_E^{sc}) \\ -[2\tilde{n} - ((k_\gamma^2\tilde{\gamma}\gamma)/n_H)](n_D/\tau_E^{sc}) \\ -[2\tilde{n} - (\gamma-1)(k_\gamma^2\tilde{\gamma})/n_H](n_T/\tau_E^{sc}) \\ -\tilde{n}(Z_I+1)(n_I/\tau_E^{sc}) \\ \tilde{n}(Z_I+1)(n/\tau_E^{sc}) \\ (Z_I+1)\tilde{n}\dot{n} \end{bmatrix}, \quad (27)$$

reduces (25) to (26). Note that $\dot{\hat{\theta}} \approx \dot{\tilde{\theta}}$ because changes in the uncertain parameters are considered to be negligible ($\dot{\theta} \approx 0$). Despite model uncertainty, adaptive control laws (21), (22), (23), (24) and (27) stabilize the equilibria of system (15).

The stability of $\tilde{n}_\alpha$ can be shown with $V_\alpha = \tilde{n}_\alpha^2/2$ which has derivative $\dot{V}_\alpha = \tilde{n}_\alpha(-\theta_3 n_\alpha/\tau_E^{sc} + S_\alpha)$. With the stabilization of $\tilde{n}$, $\tilde{\gamma}$, $\tilde{E}_i$ and $\tilde{E}_e$, the sum $(-\theta_3 n_\alpha/\tau_E^{sc} + S_\alpha)$ increases with decreasing n_α and vice versa. Therefore, it is valid to write $(-\theta_3 n_\alpha/\tau_E^{sc} + S_\alpha) = -\mu\tilde{n}_\alpha$ where μ is a positive continuous function. The stability of $\tilde{n}_\alpha$ is proven with $\dot{V}_\alpha = -\mu\tilde{n}_\alpha^2 < 0 \ \forall \ \tilde{n}_\alpha \neq 0$ when $\tilde{n} = \tilde{\gamma} = \tilde{E}_i = \tilde{E}_e = 0$. The stability of $\tilde{n}_I$ can be shown using the impurity balance (2) at steady-state, $0 = -n_I + f_I^{sp} n$. Clearly, $\tilde{n}_I = 0$ when $\tilde{n} = 0$.

V. CONTROL ALLOCATION ALGORITHM

To represent ITER, four power actuators are considered. The ion cyclotron (IC) system, electron cyclotron (EC) system and two neutral beam (NB) injectors, respectively, deliver powers P_{ic}, P_{ec}, $P_{nbi,1}$ and $P_{nbi,2}$ to the plasma. Respectively, the IC and EC systems directly heat ions and electrons by sending electromagnetic radiation at frequencies resonant with ions and electrons. Heat is then transferred between species via particle collisions (modeled using P_{ei}).

The NB power heats the plasma by injecting highly kinetic particles at a high repetition rate. Therefore, the NB injectors are sources of fast ions subject to the dynamics described by (9) through (12). The NB injectors planned for ITER will fire deuterium particles with 1 MeV of energy into the plasma [15]. Consequently, the fraction of the NB power deposited into the plasma ions, ϕ_{nbi}, is calculated using (10) and (12) with $\varepsilon_{nbi_0} = 1$ MeV and $A_{nbi} = 2$. In Section IV, the virtual control efforts $P_{aux,i}$ and $P_{aux,e}$ required for energy stabilization were obtained. The relationships between virtual control efforts and control inputs, with $\bar{\phi}_{nbi} \triangleq 1 - \phi_{nbi}$, are

$$\begin{aligned} P_{aux,i} &= \eta_{ic}P_{ic} + \eta_{nbi,1}\phi_{nbi}P_{nbi,1} + \eta_{nbi,2}\phi_{nbi}P_{nbi,2}, \quad (28) \\ P_{aux,e} &= \eta_{ec}P_{ec} + \eta_{nbi,1}\bar{\phi}_{nbi}P_{nbi,1} + \eta_{nbi,2}\bar{\phi}_{nbi}P_{nbi,2}, \end{aligned}$$

where η_{ic}, η_{ec}, $\eta_{nbi,1}$, and $\eta_{nbi,2}$ are actuator efficiency factors which can be set to zero to simulate actuator failures.

Since four actuators are available to achieve two virtual control efforts, the system is over-actuated [16]. In this section, a control allocation (CA) algorithm is designed to coordinate the actuators so that the desired virtual control efforts are produced. The algorithm considers actuator saturation and rate constraints. Separating the power of the two NB injectors in (28) allows the CA algorithm to consider fault scenarios where only one NB injector is available. The system would still be over-actuated if $\eta_{nbi,1} = \eta_{nbi,2}$ and $P_{nbi,1} = P_{nbi,2}$. The equations in (28) are rewritten as

$$v = Bu = \begin{bmatrix} \eta_{ic} & 0 & \eta_{nbi,1}\phi_{nbi} & \eta_{nbi,2}\phi_{nbi} \\ 0 & \eta_{ec} & \eta_{nbi,1}\bar{\phi}_{nbi} & \eta_{nbi,2}\bar{\phi}_{nbi} \end{bmatrix} u, \quad (29)$$
$$v = \begin{bmatrix} P_{aux,i} & P_{aux,e} \end{bmatrix}^T, \ u = \begin{bmatrix} P_{ic} & P_{ec} & P_{nbi,1} & P_{nbi,2} \end{bmatrix}^T.$$

The control effectiveness matrix, B, is state-dependent and time-varying. In the static effector model (29), B is updated at every sampling instant. The algorithm's primary objective is to calculate the control input u that produces the virtual efforts requested by the controller. When this objective fails due to actuator constraints, the algorithm searches for a u that minimizes the allocation errors (differences between the requested virtual efforts and the efforts produced by the constrained actuators). A secondary objective is to minimize the total power consumed by the heating systems.

Respectively, $\bar{u}$ and $\underline{u}$ contain the upper and lower saturation limits of each actuator. For ITER, the IC system, the EC system and each of the NB injectors will have a maximum power of 20 MW, 20 MW and 16.5 MW, respectively [2]. The minimum power is zero for each actuator. The upper and lower rate constraints are placed into $\bar{\delta}$ and $\underline{\delta}$, respectively. Then, the most restrictive lower and upper limits are

$$u_l = \max(\underline{u}, u^\star + \Delta t\underline{\delta}), \quad u_u = \min(\bar{u}, u^\star + \Delta t\bar{\delta}), \quad (30)$$

where $u^\star$ is the control input from the last sampling instant, Δt is the time step, and the elements of $\underline{\delta}$ are negative.

The CA problem is posed as a quadratic program (QP):

$$\begin{aligned} \underset{s,u}{\text{minimize}} \quad & \left(\sum_{i=1}^{2} g_i s_i^2 + \sum_{j=1}^{4} w_j u_j^2\right) \\ \text{subject to} \quad & Bu = v + s, \quad u_l \leq u \leq u_u. \end{aligned} \quad (31)$$

The slack variables $s = \begin{bmatrix} s_1, \ s_2 \end{bmatrix}^T$ are introduced to allow error in the mapping between u and v due to actuator constraints [17]. The elements of g and w are set to 10^4 and 1, respectively, because minimizing the slack variables takes priority over minimizing the total power consumption.

Problem (31) is reformulated as a standard QP:

$$\underset{s,u}{\text{minimize}} \quad \frac{1}{2}(u^T, s^T)H\begin{pmatrix}u\\ s\end{pmatrix} \tag{32}$$
$$\text{subject to} \quad (B, -I)\begin{pmatrix}u\\ s\end{pmatrix} = v, \quad \begin{pmatrix}I & 0\\ -I & 0\end{pmatrix}\begin{pmatrix}u\\ s\end{pmatrix} \geq \begin{pmatrix}u_l\\ -u_u\end{pmatrix},$$

where $H = 2 \times diag(w_1, ..., w_4, g_1, g_2)$. The introduction of slack variables ensures the existence of a feasible solution. Since H is positive definite, the QP is a strictly convex optimization problem with a unique optimal solution [18].

Fueling CA is not required because ITER will only have two pellet injectors to supply S_D and S_T. Maximum fueling rates will be $S_D = 120$ Pa m^3/s and $S_T = 111$ Pa m^3/s [2].

VI. SIMULATION STUDY

The performance of the adaptive control and control allocation (CA) algorithms are assessed with the following simulation study. For comparison with CA scheme (32), a simpler CA scheme is introduced. The least-squares problem,

$$\underset{u}{\text{minimize}} \ (1/2)u^T I u \quad \text{subject to} \quad Bu = v, \tag{33}$$

has the solution $u = B^+ v$ where $B^+ = B^T(BB^T)^{-1}$ is the Moore-Penrose pseudo-inverse. Actuator constraints (30) are applied after solving (33).

Three 270 second simulations with different burn control and CA schemes are compared. All simulations use control laws (21), (22), (23) and (24). An adaptive controller (adaptive law (27)) with QP CA (32) is compared to a non-adaptive ($d\hat{\theta}/dt = 0$) controller with QP CA to test the adaptive control algorithm. To assess the effectiveness of the QP CA algorithm (32), the adaptive controller with QP CA is also compared to an adaptive controller with pseudo-inverse CA (33). Each simulation used $n_\alpha = 2.6 \times 10^{18}$m^{-3}, $n_D = 4.2 \times 10^{19}$m^{-3}, $n_T = 4.5 \times 10^{19}$m^{-3}, $n_I = 1 \times 10^{18}$m^{-3}, $E_i = 2.05 \times 10^5$J/m^3 and $E_e = 2.4 \times 10^5$J/m^3 as initial conditions (also $Z_I = 4$). The nominal values (and initial control estimates) of uncertain parameters H, ζ_i, ζ_e, k_α, k_D, k_T, k_I and f_I^{sp} were 1.1 (1.02), 1.15 (1.25), 0.85 (1), 6 (8.2), 3 (4), 2.5 (4), 8.7 (12) and 0.005 (0.02), respectively. Actuator saturation limits were given in Section V. The IC, EC and NB rate constraints were taken to be ± 10 MW/s, ± 10 MW/s and ± 1 MW/s, respectively. The heating efficiencies were set to η_{ic}=0.9, η_{ec}=0.9, $\eta_{nbi,1}$=1 and $\eta_{nbi,2}$=0.8. The desired equilibrium initially given to the controllers was determined by using $\bar{E}_i$=1.83×10^{5}J/m^3, $\bar{E}_e$=2.4×10^{5}J/m^3, $\bar{n} = 2 \times 10^{20}$m^{-3} and $\bar{\gamma} = 0.5$ to solve (14) with $d/dt = 0$ and nominal θ. At 90 seconds, the desired equilibrium was changed to that defined by $\bar{E}_i = 1.65 \times 10^5$J/m^3, $\bar{E}_e = 2.15 \times 10^5$J/m^3, $\bar{n} = 1.8 \times 10^{20}$m^{-3} and $\bar{\gamma} = 0.48$. The CA modules were evaluated with an actuator fault scenario. At 180s, the second NB injector shuts down. This was simulated by setting its efficiency ($\eta_{nbi,2}$) to zero, its saturation limit to zero, and allowing it to drop to zero instantly.

Fig. 1 (a, b, c, d) demonstrates how well the three control schemes track target equilibria using the actuation shown in Fig. 2. Due to uncertainties, the non-adaptive controller with QP CA moves the system away from the targets. The adaptive controller with QP CA successfully stabilizes the desired equilibria despite the uncertainties and actuator fault. In the first two-thirds of the simulation, both CA schemes favor the first NB injector over the second due to its better efficiency. Despite the actuator fault at 180s, the adaptive controller with QP CA holds the system at the desired ion and electron energy targets, while the adaptive controller with pseudo-inverse CA cannot keep the system on the targets.

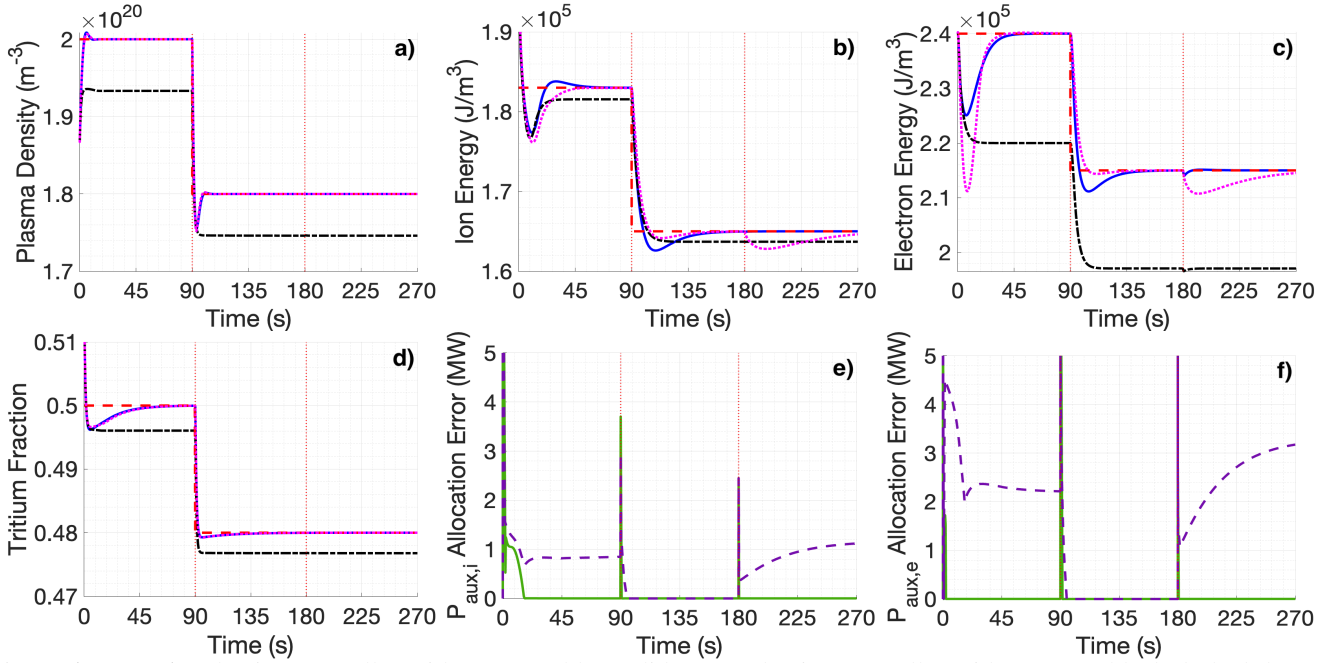

Fig. 1: **(a, b, c, d)** Adaptive controller with QP CA (blue solid), non-adaptive controller with QP CA (black dashed-dotted) and adaptive controller with pseudo-inverse CA (magenta dotted) attempt to track targets (red dashed). **(e, f)** Allocation errors under adaptive control with QP CA (green solid) and pseudo-inverse CA (purple dashed) are compared.

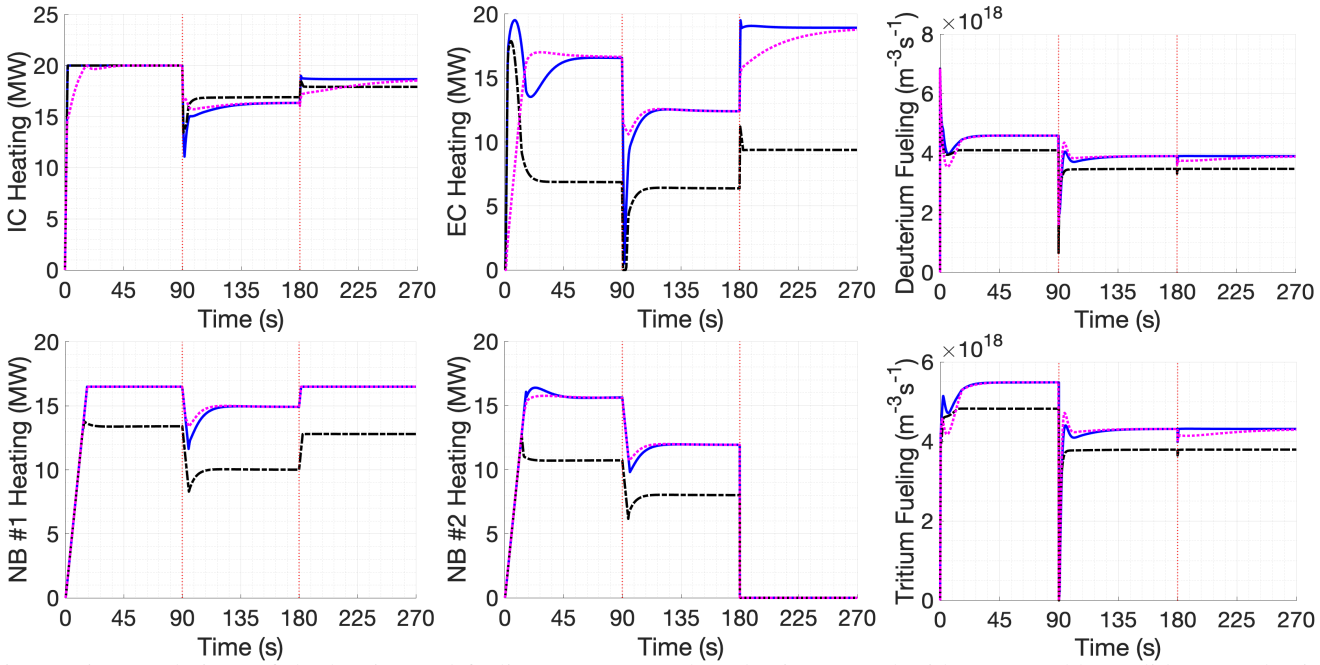

Fig. 2: Time evolutions of the heating and fueling actuators under adaptive control with QP CA (blue solid), non-adaptive control with QP CA (black dashed-dotted) and adaptive control with pseudo-inverse CA (magenta dotted) are presented.

The allocation errors produced by the adaptive controller with QP CA and pseudo-inverse CA are compared in Fig. 1 (e, f). The allocation errors are the absolute values of the differences between the requested control efforts (calculated from (21) and (22)) and the efforts produced from the allocated actuators (calculated from (28) after solving either (32) or (33)). Allocation errors occur because either the requested efforts are unattainable due to actuator constraints or the CA module fails to find a solution to (29). Throughout the simulation, the QP CA scheme finds a solution with zero allocation errors. The pseudo-inverse CA scheme misses the requested efforts by a few megawatts in both the first-third and last-third of the simulation. The failure of the pseudo-inverse CA scheme to meet the requested external heating generates steady-state errors in the ion and electron energies. Measured at 270s, the steady-state errors are $|\Delta E_i| = 1.12 \times 10^5$J and $|\Delta E_e| = 1.42 \times 10^5$J. With QP CA, the steady-state errors are negligible ($|\Delta E_i| = 2.5$J and $|\Delta E_e| = 20.4$J). Clearly, the more complex QP CA module is worth the extra design effort and computational load.

VII. CONCLUSIONS AND FUTURE WORK

The proposed nonlinear adaptive burn control algorithm successfully determines the virtual control efforts that force the plasma to equilibrium targets despite the model uncertainties. The actuator redundancy of the two-temperature plasma is resolved with a control allocator that determines the constrained inputs that best achieve the requested virtual control efforts. Future work may focus on adaptive control allocation to manage the existence of uncertain parameters in the effector model (29). Another problem to consider is the inclusion of time delays in the model. Time delays, such as actuator response times and the ablation time of injected fuel pellets, can degrade the closed-loop performance.

REFERENCES

[1] J. Wesson, *Tokamaks*, 2nd ed. Oxford: Clarendon Press, 1997.

[2] J. A. Snipes *et al.*, "Actuator and diagnostic requirements of the ITER plasma control system," *Fusion Eng. and Design*, vol. 87, no. 12, 2012.

[3] E. Schuster, M. Krstic, and G. Tynan, "Burn control in fusion reactors via nonlinear stabilization techniques," *Fusion Science and Technology*, vol. 43, no. 1, pp. 18–37, 2002.

[4] M. D. Boyer and E. Schuster, "Nonlinear control and online optimization of the burn condition in ITER via heating, isotopic fueling and impurity injection," *Plasma Phys. and Control. Fusion*, vol. 56, no. 10, 2014.

[5] V. Graber and E. Schuster, "Nonlinear adaptive burn control of two-temperature tokamak plasmas," in *IEEE Conference Decision and Control*, Nice, France, 2019.

[6] M. Shimada *et al.*, "Physics design of ITER-FEAT," *J. Plasma Fusion Res.*, vol. 3, pp. 77–83, 2000.

[7] J. Hansen and I. McDonald, "Thermal relaxation in a strongly coupled two-temperature plasma," *Physics Letters A*, vol. 97, no. 1-2, pp. 42–44, 1983.

[8] H. Khalil, *Nonlinear Systems*, 3rd ed. New Jersey: Prentice Hall, 2001.

[9] O. Härkegård and S. T. Glad, "Resolving actuator redundancy - optimal control vs. control allocation," *Automatica*, vol. 49, pp. 1087–1103, 2013.

[10] H. S. Bosch and G. M. Hale, "Improved formulas for fusion cross-sections and thermal reactivities," *Nucl. Fusion*, vol. 32, no. 4, 1992.

[11] R. Gross, *Fusion Energy*. New York: Wiley-Interscience, 1984.

[12] D. Gallart, M. Mantsinen, and Y. Kazakov, "Modelling of ICRF heating in DEMO with special emphasis on bulk ion heating," in *AIP Conference Proceedings*, vol. 1689, no. 1, 2015.

[13] M. Shimada *et al.*, "Chapter 1: Overview and summary," *Nucl. Fusion*, vol. 47, 2007.

[14] Krstić, Kanellakopoulos, and Kokotović, *Nonlinear and Adaptive Control Design*. Wiley, 1995.

[15] R. S. Hemsworth *et al.*, "Overview of the design of the ITER heating neutral beam injectors," *New J. Phys.*, vol. 19, 2017.

[16] M. W. Oppenheimer, D. B. Doman, and M. A. Bolender, "Control allocation for over-actuated systems," in *2006 14th Mediterranean Conference on Control and Automation*, Ancona, 2006.

[17] T. A. Johansen and T. I. Fossen, "Control allocation - a survey," *Automatica*, vol. 49, pp. 1087–1103, 2013.

[18] S. Boyd and L. Vandenberghe, *Convex Optimization*. Cambridge University Press, 2004.